

## PARAMETER SENSITIVITY STUDY OF BOILING AND TWO-PHASE FLOW MODELS IN COMPUTATIONAL THERMAL HYDRAULICS

I. M. Asher<sup>2</sup>, T. J. Drzewiecki<sup>1</sup>, K. J. Fidkowski<sup>2</sup>, and T. J. Downar<sup>1</sup>

<sup>1</sup> Department of Nuclear Engineering and Radiological Sciences

<sup>2</sup> Department of Aerospace Engineering

University of Michigan, Ann Arbor

[isaaca@umich.edu](mailto:isaaca@umich.edu), [tjdrzew@umich.edu](mailto:tjdrzew@umich.edu), [kfid@umich.edu](mailto:kfid@umich.edu), [downar@umich.edu](mailto:downar@umich.edu)

### Abstract

This work presents a sensitivity study of boiling and two phase flow models for thermal hydraulics simulations in nuclear reactors. The study quantifies sources of uncertainty and error in these simulations by computing global sensitivities of figures of merit, or outputs, to model parameters, inputs, and mesh resolution. Results are obtained for the DEBORA benchmark problem of boiling in a channel driven by a heated wall section. Scalar outputs of interest are average wall temperature, integrated cross-sectional void fraction, and pressure drop in the channel. Sensitivities are computed with respect to both individual heat fluxes and to the parameters in the models for these heat fluxes.

### 1. Introduction

Models for boiling and two-phase flows, particularly in the subcooled regime, are important for thermal hydraulics simulations that support safety and performance analyses of nuclear reactors. Numerous models are currently available for such simulations, e.g. [1,2], many with first-principles justifications [3], but each with a certain number of parameters that can be regarded as tunable or empirically-based. In some cases, these models do not give the same answers and do not necessarily correlate to experiments if they are not independently adjusted for the particular case of interest. A documented example is the failure of high-pressure models applied to subcooled boiling at low pressures [4].

The objective of this study is to take a first step towards quantifying uncertainties in thermal hydraulics simulations by systematically computing global sensitivities of figures of merit, or outputs, to model parameters and inputs. These sensitivities are used to identify parameters that are important for the prediction of the outputs of interest, allowing for a reduction of the input-space dimensionality in future applications such as uncertainty propagation and reliability analysis. Furthermore, for parameters identified as important, the computed sensitivities can be combined with a priori estimates of parameter uncertainty and variability to identify critical parameters and suggest areas of model improvement.

Previous works have considered the sensitivity of boiling models to inputs parameters and sub-models. Tu and Yeoh [5] studied subcooled boiling at low pressure using Ansys CFX and found that parameters pertaining to partitioning of the wall heat flux, the mean bubble diameter, and the bubble departure diameter have a strong effect on the void fraction. Koncar and Krepper [6] used Ansys CFX to investigate boiling of a refrigerant in turbulent subcooled boiling, for which sufficient mesh resolution,

the correct bubble diameter, and the inclusion of the bubble lift force were found to be important for ensuring accurate validation.

This sensitivity study proceeds by choosing representative boiling and two-phase flow models in the Eulerian Multiphase CFD code STAR-CD [7]. The DEBORA test case, which consists of subcooled boiling in a straight channel geometry with simple boundary conditions, is the benchmark problem that drives this study. The STAR-CD code has been used for validating subcooled boiling models in previous work [8]. The scalar outputs of interest in the present study are the average wall temperature, an integrated void fraction at one axial location, and the pressure drop in the channel. Input parameters pertaining to one aspect of the boiling simulations, the wall-to-flow heat transfer model, are varied in a systematic fashion using design-of-experiment capability in the software package DAKOTA. This package is also used to post-process the results. In addition, effects of mesh size on the outputs are investigated using a sequence of three mesh resolutions.

## 2. CFD Two Phase Models and Constitutive Relations

The STAR-CD Eulerian two-phase solver tracks the mass, momentum, and energy of the liquid and vapour phases in each computational cell. A modified  $k$ - $\epsilon$  model is used to model the turbulence in the continuous phase, with an algebraic formula used to model the turbulence in the dispersed phase. Full details of the Eulerian two-phase flow models in STAR-CD can be found in the STAR-CD manual [7]. The mass, momentum, and energy transport equations are given below.

$$\text{Mass} \quad \frac{\partial}{\partial t}(\alpha_k \rho_k) + \nabla \cdot (\alpha_k \rho_k \mathbf{u}_k) = \sum_{j=1}^N (\dot{m}_{jk} - \dot{m}_{kj}) \quad (1)$$

$$\text{Momentum} \quad \frac{\partial}{\partial t}(\alpha_k \rho_k \bar{\mathbf{u}}_k) + \nabla \cdot (\alpha_k \rho_k \bar{\mathbf{u}}_k \bar{\mathbf{u}}_k) = -\alpha_k \nabla p + \alpha_k \rho_k \bar{\mathbf{g}} + \nabla \cdot \alpha_k (\boldsymbol{\tau}_k + \boldsymbol{\tau}'_k) + M_k \quad (2)$$

$$M = F_D + F_{TD} + F_L + F_{VM} + \sum_{j=1}^N (\dot{m}_{jk} \bar{\mathbf{u}}_j - \dot{m}_{kj} \bar{\mathbf{u}}_k) \quad (3)$$

$$\text{Energy} \quad \frac{\partial}{\partial t}(\alpha_k \rho_k h_k) + \nabla \cdot (\alpha_k \rho_k \bar{\mathbf{u}}_k h_k) - \nabla \cdot \left[ \alpha_k \left( \lambda_k \nabla T_k + \frac{\mu_t}{\sigma_h} \nabla h_k \right) \right] = Q_k \quad (4)$$

$$Q_k = \alpha_k \frac{Dp_k}{Dt} + \alpha_k (\boldsymbol{\tau}_k + \boldsymbol{\tau}'_k) : \nabla \bar{\mathbf{u}}_k + \sum_{i \neq k} Q_{ki} + \sum_{(ik)} Q_k^{(ik)} + \sum_{i \neq k} (m_{ki} h_k^{(ik)} - m_{ik} h_k) \quad (5)$$

Additional constitutive equations are implemented in order to close the model. These relationships can be classified into areas of phase-to-phase momentum transfer, phase-to-phase heat and mass transfer, and wall-to-flow heat transfer.

### Phase-to-phase momentum transfer

From Eq. 3, models are needed to determine the drag force,  $F_D$ , turbulent dispersion force,  $F_{TD}$ , the lift force,  $F_L$ , and the virtual mass force,  $F_{VM}$ . The drag force is calculated using Eq. 6, where the coefficient,  $A_D$ , and relative velocity is,  $\mathbf{u}_r$ , are given by Eq. 7 and Eq. 8 respectively.

$$F_D = A_D \bar{\mathbf{u}}_r \quad (6)$$

$$A_D = \frac{3}{4} \frac{\alpha_d \rho_c C_D}{d} |\bar{\mathbf{u}}_r| \quad (7)$$

$$\bar{\mathbf{u}}_r = \bar{\mathbf{u}}_c - \bar{\mathbf{u}}_d \quad (8)$$

Determination of the bubble drag coefficient is obtained using the correlation of Wang [9], given by Eq. 9 and the coefficients provided in [9], with  $a, b, c$  dependent on  $Re_d$ .

$$C_D = \exp\left[a + b \ln Re_d + c(\ln Re_d)^2\right] \quad (9)$$

The turbulent dispersion force is given by Eq. 10 and utilizes terms previously defined for the determination of the drag force. The turbulent Prandtl number is set to 1.0.

$$F_{TD} = -A_D \frac{v'_c}{\sigma_\alpha} \left[ \frac{\nabla \alpha_c}{\alpha_c} - \frac{\nabla \alpha_d}{\alpha_d} \right] \quad (10)$$

The lift force is given by Eq. 11 with the lift coefficient,  $C_L$ , set to -0.03.

$$F_L = C_L \alpha_d \rho_c [\vec{u}_r \times (\nabla \times \vec{u}_r)] \quad (11)$$

The virtual mass force is calculated using Eq. 12 with a virtual mass coefficient of 0.5.

$$F_{VM} = C_{VM} \alpha_d \rho_c \left[ \frac{D\vec{u}_c}{Dt} - \frac{D\vec{u}_d}{Dt} \right] \quad (12)$$

#### *Phase-to-phase heat and mass transfer*

Heat transfer from the liquid to the bubble interface is determined using Eq. 13, where the heat transfer coefficient is determined using the model of Ranz and Marshall [10], see Eq. 14.

$$\dot{q}_l = h_l A_d (T_l - T_{sat}) \quad (13)$$

$$Nu_l = 2 + 0.6 Re_d^{0.5} Pr_l^{0.3} \quad (14)$$

A similar relationship is used for the heat transfer from the vapour to the bubble interface, see Eq. 15. However, the heat transfer coefficient is obtained by using a constant Nusselt number of 26.

$$\dot{q}_g = h_g A_d (T_g - T_{sat}) \quad (15)$$

The relationships for phase-to-phase heat transfer are then utilized to determine the water to steam mass transfer rate given by Eq. 16.

$$\dot{m} = (\dot{q}_l + \dot{q}_g) / h_{fg} \quad (16)$$

In determining the phase-to-phase heat transfer, the interfacial area concentration is required. In place of a more sophisticated treatment for interfacial area, such as the interfacial area transport model developed by Ishii [11], the interfacial area concentration is obtained by utilizing the void fraction and Sauter mean diameter. This expression is given by Eq. 17.

$$A_d = 6\alpha_g / d \quad (17)$$

In a manner similar to Kurul and Podowski [1] it is assumed that the bubble diameter is a function of the local liquid subcooling. The expression for the Sauter mean diameter is given by Eq. 18 with  $d_0=0.15$  mm,  $d_l=2$  mm,  $\Delta T_0=13.5$  K, and  $\Delta T_l=-5$  K.

$$d = \frac{d_1(\Delta T_{sub} - \Delta T_0) + d_0(\Delta T_1 - \Delta T_{sub})}{(\Delta T_1 - \Delta T_0)} \quad (18)$$

### Wall-to-flow heat transfer

The heat transfer from the wall to the fluid in subcooled boiling consists of three parts: single phase convective heat transfer, evaporative heat transfer, and the quenching heat transfer (see Eq. 19).

$$q_T'' = q_c'' + q_e'' + q_q'' \quad (19)$$

The evaporative heat flux is obtained using Eq. 20, where  $n''$  is the nucleation site density and  $f$  is the bubble departure frequency.

$$q_e'' = \frac{\pi d_w^3}{6} \rho_g h_{fg} f n'' \quad (20)$$

The nucleation site density is obtained using Eq. 21 with  $m=185.0$  and  $p=1.805$ , and the bubble departure frequency is obtained using Eq. 22.

$$n'' = (m \Delta T_{sup})^p \quad (21)$$

$$f = \sqrt{\frac{4g(\rho_l - \rho_g)}{3d_w \rho_l}} \quad (22)$$

The wall is broken up into two regions:  $A_e$  is the area fraction where evaporative heat transfer occurs and  $A_c$  is the area fraction where single phase convective heat transfer occurs. The area fraction of evaporative heat transfer is determined using Eq. 23, with the coefficient,  $F_A$ , set to 2.0.

$$A_e = F_A \left( \frac{\pi}{4} d_w^2 \right) n'' \quad (23)$$

With the evaporative area fraction, the single-phase convective heat flux and quenching heat flux are obtained using Eq. 24 and Eq. 25, respectively. The single-phase heat transfer coefficient is obtained using wall functions associated with the  $k-\varepsilon$  turbulence model. The quenching heat transfer coefficient is obtained using the model of Del Valle and Kenning, Eq. 26, with wait time determined by Eq. 27.

$$q_c'' = h_c (1 - A_e) (T_{wall} - T_l) \quad (24)$$

$$q_q'' = h_q A_e (T_{wall} - T_l) \quad (25)$$

$$h_q = 2f \sqrt{t_w \rho_l C_{p,l} \lambda_l / \pi} \quad (26)$$

$$t_w = 0.8 / f \quad (27)$$

A bubble departure size is needed to determine the evaporative heat flux and evaporative area fraction. The expression of Tolubinsky and Kostanczuk [12], obtained for water at a liquid velocity of 0.2 m/s, is utilized. This expression, given by Eq. 28, utilizes a coefficient,  $d_0$ , of 0.6 mm which is modified from the original value of 1.4 mm. A value for  $\Delta T_0$  of 45 K is consistent with the original reference.

$$d_w = d_0 \exp(-\Delta T_{sub} / \Delta T_0) \quad (28)$$

### 3. Test case and applications

One of the CASL T/H challenge problems involves using CFD to identify regions where subcooled boiling can occur. Therefore, a test case was chosen to assess the performance of CFD to model subcooled boiling. The DEBORA experiment was performed at the Commissariat à l'Énergie Atomique. In this experiment, R-12 is used as the working fluid to simulate pressurized water reactor conditions under low pressure. Liquid R-12 flows upward inside a vertical pipe having an internal diameter equal to 19.2 mm. The whole pipe can be divided axially into three parts: the adiabatic inlet section (1 m length), the heated section (3.5 m length), and the adiabatic outlet section ( $\approx 0.5$  m length). Vapor bubbles are generated by nucleation onto the wall surface and condense into the subcooled liquid when they are far from the wall. In this experiment, local measurements can be performed with a sensor displaced in the radial direction only [13]. At the end of the heated section, the radial profiles of the void fraction and bubble diameter have been measured by means of an optical probe, and liquid temperature has been measured by thermocouples.

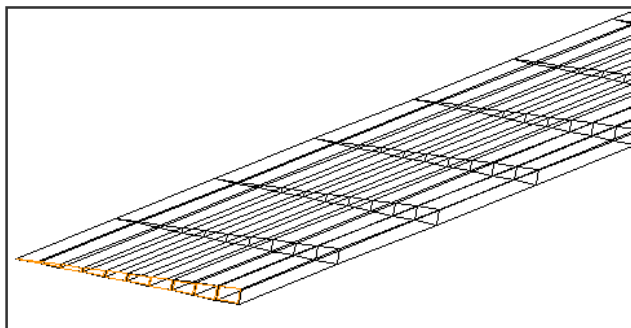


Figure 1. Portion of the mesh used in the STAR-CD model

The STAR-CD model of the DEBORA experiment utilizes an axisymmetric mesh, a portion of which is shown in Fig. 1. In order to investigate mesh sensitivity test cases were run on eight different mesh sizes, all uniformly spaced along each dimension. The system pressure is 1.459 MPa with inlet conditions specified at an inlet velocity of 1.72 m/s and void fraction of 0.001. The wall heat flux is 76.24 kW/m<sup>2</sup>. Implementation of the wall-to-fluid heat transfer models is accomplished through the use Fortran subroutines that are implanted into STAR-CD through user-

defined “ufiles” [7].

### 4. Uncertainty quantification methods and codes

A Monte-Carlo approach was used to perform the sensitivity analysis in which several simulations are run at various combinations of the uncertain parameters. The results of those simulations were then used to estimate the sensitivity of outputs of interest to the uncertain parameters. Latin-Hypercube sampling, which attempts to ensure that the parameter space is fully explored, was used to determine the appropriate values of the parameters to simulate.

For each parameter, a prior probability distribution was assumed. In this case, the parameters were unknown model variables for which experimental data was not available to provide a distribution. For the purpose of the sensitivity study, each parameter was assumed to have a uniform probability density function within a small range around a nominal value. The nominal value was the value given in the original implementation of the STAR-CD two-phase flow model.

With these assumed probability distributions, each parameter range was discretized into  $n$  quantiles, which were regions of equal probability. Latin-Hypercube samples ensure that, for each parameter, each quantile has an equal number of samples. The samples within the quantiles were chosen according to the probability distribution, which in this case was uniform. A balanced experiment can

be obtained by constraining the total number of samples to be an integer multiple of  $pn$ , where  $p$  is the number of parameters. A sample set of samples for a two-parameter study is shown in Fig. 2.

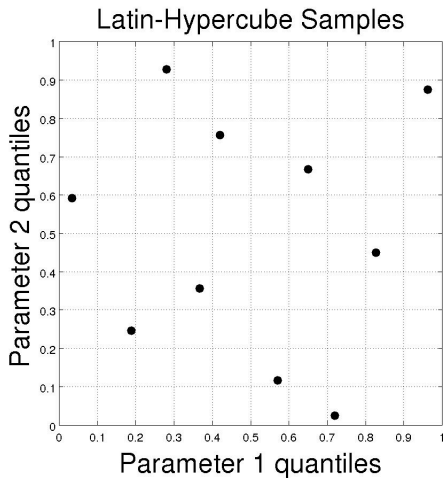


Figure 2. Representative Latin-Hypercube samples for a two parameter study

Once these samples were chosen, the simulation was run for each sample, i.e. for each combination of the model parameters. The outputs were then computed and the sensitivities were estimated.

The approach used here assumes continuous variation of the parameters, and therefore an alternative formulation was required for discrete parameters. In this case, the only discrete parameter was the mesh resolution, since three representative meshes were used to compute the solutions. In general for discrete uncertain parameters, only numerical values of main and interaction effects were available, whereas continuous parameters produce distributions. The mesh resolution parameter was further unique

because it did not represent an underlying physical uncertainty. It was chosen by the modeler based on experience, which could not be modeled with a fixed probability distribution. It was therefore necessary to re-run the entire study for each choice of mesh. However, in order to use a consistent framework, the mesh resolution parameter was formulated as a discrete random variable with a uniform distribution. Since Latin-Hypercube samples were used, the subset of samples with a given mesh resolution also formed a valid Latin-Hypercube sampling set for the remaining uncertain variables.

Choosing which parameters to vary was to some extent an ad-hoc process, since each model had various uncertain empirical constants (one could also say that the mathematical forms were uncertain, but this possibility was not explored in this study). A hierarchical approach was used and the overall boiling model was divided into sub-models. For example, STAR-CD assumes that the heat flux at a wall can be divided into components due to evaporation, convection, and quenching. The equation for the evaporative heat transfer (Eq. 19) is then treated as a sub-model, and there are even finer levels of models. In the case of evaporative heat transfer, there are finer models for the bubble diameter at the wall and the nucleation site density.

In the sensitivity study, the highest level models were varied first, followed sequentially by finer models. Thus, important parameters for the entire STAR-CD model were uncovered. The study began by varying the various heat transfer rates by  $\pm 30\%$ . A large sensitivity would then prompt a study of the parameters of the sub-model. If one of the high-level parameters did not influence the output of interest, the associated sub-model could be safely ignored.

We note that any magnification of uncertainties in sub-models was ignored. That is, a variation in heat transfer of  $\pm 30\%$  may imply a variation of some empirical constant by 0.001%, or possibly 200%, depending on the structure of the sub-model. The fixed percentage variation was used in the absence of comprehensive a priori information about the ranges of the model parameters.

The Sandia DAKOTA sensitivity and uncertainty analysis software was used to generate the Latin-Hypercube samples and execute STAR-CD with the modified parameters. Continuous model parameters were treated as continuous random variables, uniform over the indicated range. Mesh

resolution was treated as a uniform discrete random variable. STAR-CD only provides point-wise outputs, and these were stored in text files that were post-processed to yield the integrated outputs of interest. The integration was performed using a third order method for the evenly-spaced points in the axial direction. In the radial direction, the mesh size varies, so the simpler midpoint method was used.

## 5. Results

### 5.1 Parameter Choice

The goal of this study was to assess the predictive power of STAR-CD, with emphasis on boiling and CRUD prediction. To that end, three outputs relevant to CRUD formation were studied: the pressure drop from inlet to outlet, the average wall temperature (over the entire length), and the average void fraction at the end of the heated section. Although there were many approximate models in the STAR-CD formulation, only the subcooled boiling wall to flow heat transfer model was investigated (Eqs. 19-28). This model interacted with the rest of STAR-CD by generating vapor (bubbles) and heating the vapor and fluid at the wall.

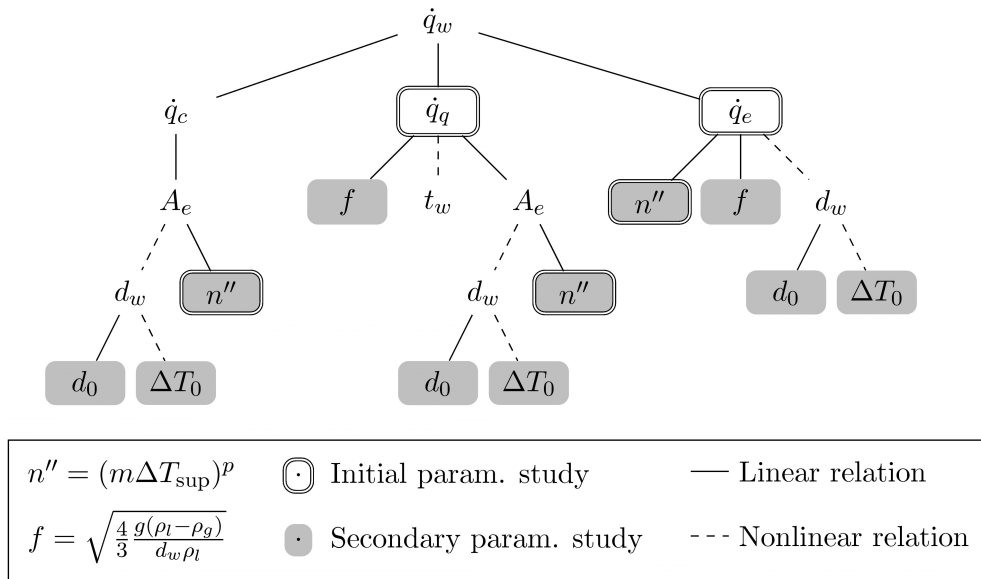


**Figure 3. STAR-CD sub-cooled boiling model hierarchy**

The model for bubble formation was very simple, so most of the subcooled boiling model was devoted to calculating heat fluxes. These heat fluxes in Eq. 19 depended on parameters like bubble size, nucleation site density, bubble departure frequency, etc. as shown in Fig. 3. Note that the departure frequency depended weakly on the bubble size. In the figure, a node corresponds to a quantity that was calculated using its children. In STAR-CD, every instance of a parameter (for example each  $d_w$ ) was calculated with the same routine.

### 5.2 Mesh Convergence

Eight different meshes were used to investigate the sensitivity of the three chosen outputs to mesh resolution. The mesh sizes included: 60x6x1, 80x8x1, ..., 200x20x1 (axial by radial by azimuthal) all of the same family. The resulting convergence of outputs is shown in Fig. 4.

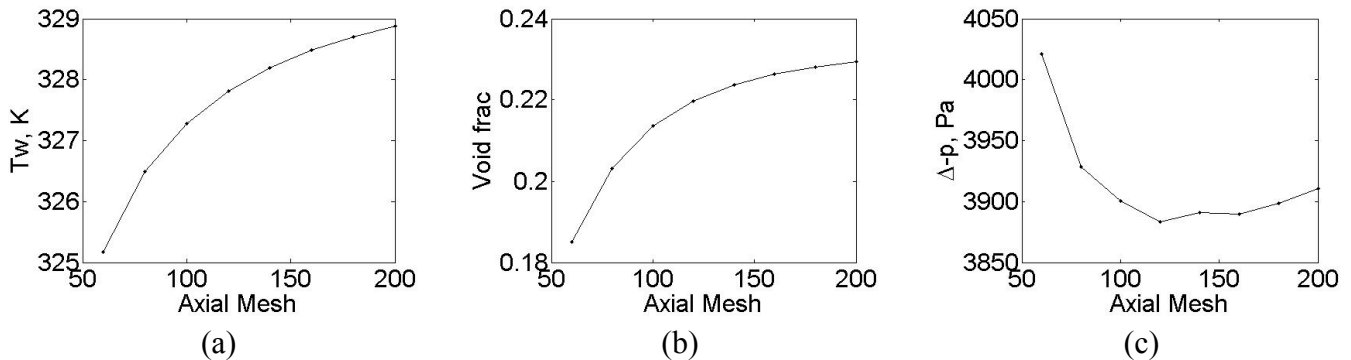
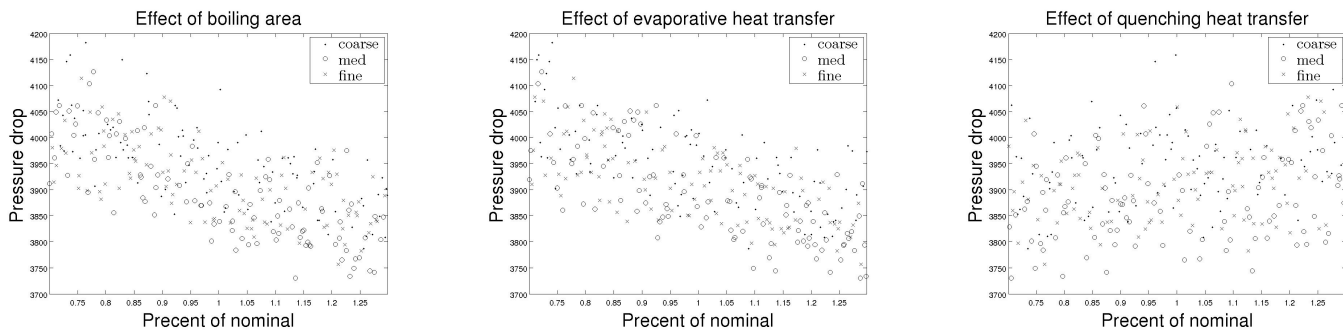


Figure 4. Mesh sensitivity of (a) average wall temperature, (b) void fraction at end of heated section, and (c) pressure drop across pipe.

The results do not demonstrate ideal asymptotic convergence, in particular for the pressure drop, but the variations are not excessive, and due to relatively long run times further mesh refinement was not performed. Instead three mesh resolutions were chosen for the sensitivity study: 80x8x1 (coarse), 120x12x1 (medium), and 180x18x1 (fine).

### 5.3 Three Parameter Study

High-level models were varied first, which involved coefficients on  $q_c$ ,  $q_q$ , and  $q_e$ . Due to restrictions in the way the code calculates these heat fluxes, it was practical to instead vary  $n$ ,  $q_q$ , and  $q_e$ . Since  $n$  was used (linearly) in all three heat fluxes, effects due to variations in any of the  $q$  are discernable. The quantities were varied by  $\pm 30\%$  and there were 298 total samples (approximately Latin-Hypercube), each of which converged to an absolute residual of  $10^{-5}$ . Fig. 5 shows plots of each output against variations in one of the inputs, for each of three meshes. The correlation coefficients of the inputs and outputs are shown in Table 1. Note that the coefficients for the physically relevant random parameters (not mesh size) were calculated for the fine mesh only. The coefficient for mesh size was calculated by assuming that mesh size was random, with smaller mesh size corresponding to the coarse mesh.



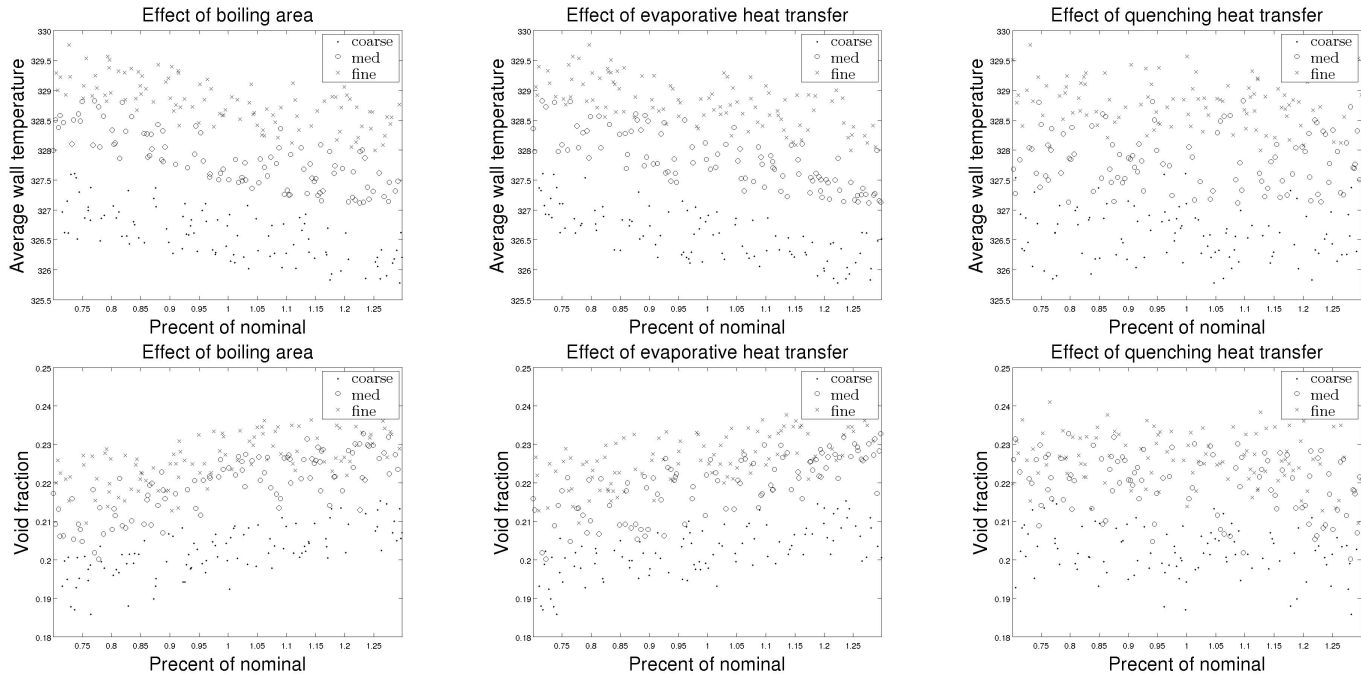


Figure 5. Sensitivity of outputs to boiling area, evaporative heat transfer, and quenching heat transfer

	$n''$	$q_e$	$q_q$	mesh size
$\Delta p$	-0.612	-0.657	0.277	-0.183
$T_w$	-0.680	-0.644	-0.125	0.905
$\alpha_g$	0.647	0.645	-0.221	0.808

Table 1. Correlation of inputs and outputs

$\Delta p - T_w$	$\Delta p - \alpha_g$	$T_w - \alpha_g$
0.914	-0.997	-0.937

Table 2. Cross-correlation of outputs

### Pressure Drop

The pressure drop across the channel was most strongly affected by boiling area (note that  $n''$  directly scales the boiling area  $A_e$ ) and evaporative heat transfer. The decrease in pressure drop was likely due to the change in hydrostatic pressure when the void fraction increased due to the increased boiling. Increases in boiling area,  $n''$ , and evaporative heat transfer both increased the amount of boiling in the channel. Although more boiling increased friction losses, which would increase the pressure drop, the data show that this effect was small compared to the change in hydrostatic pressure. The channel was quite tall (5 meters), so most of the pressure drop was due to gravity.

Heat transfer due to quenching had little effect on the pressure drop. Quenching affected the liquid temperature only, but a slightly higher or lower liquid temperature did not affect boiling, since most boiling occurred by direct heat transfer from the wall to bubbles.

### Wall Temperature

Unlike pressure drop, average wall temperature was seen to be sensitive to the mesh size. STAR-CD uses a finite-volume formulation, where quantities are averaged over cells. Cells adjacent to the wall on coarse meshes had lower temperatures than the boundary cells on finer meshes, since the finite-volume averaging process smoothed out the temperature profile. Finally, since wall heat flux was

fixed, a higher liquid temperature adjacent to the wall resulted in a higher wall temperature. Thus finer meshes had higher wall temperatures, as seen in the figures above.

In interpreting the figures, it is important to remember that mesh size is not considered random, so the variability should be assessed for each mesh individually. It is clear that boiling area and evaporative heat transfer had the strongest effect on wall temperature. This was likely due to the fact that the heat transfer coefficient was much higher from the wall to vapor than to liquid. Again, quenching did not contribute much to the overall  $q_T$ , so it was not important for wall temperature in this case.

### **Void Fraction**

The results for void fraction were similar to those of pressure drop, except that void fraction was more strongly mesh-dependent. This was expected because void fraction was a more local quantity, averaged over a single axial plane, as opposed to pressure drop, which was affected by the entire mesh. In addition, the correlation between void fraction and pressure drop from Table 2 implies that the mesh dependence is not significant compared to the effects of boiling area and heat transfers.

From the initial study, it was clear that boiling area and evaporative heat transfer strongly affected all of the outputs. Mesh size has a strong effect on wall temperature and void fraction, but a much weaker effect on pressure drop. Nonetheless, all of the outputs were highly correlated to each other. This was expected, since similar physical mechanisms are responsible for all of the output variations. Finally, quenching has a much smaller effect than any other input. Since the boiling area and evaporative heat transfer have similar correlation coefficients across all of the outputs (see Table 1), it can be deduced that it is only  $n''$  in the model for  $q_e$  that is important in this case, compared to  $q_c$  and  $q_q$ . This suggests that the evaporative heat transfer model deserves more attention.

## **5.4 Four Parameter Study**

A secondary parameter study was performed to further investigate the effects revealed by the three parameter study. From the conclusions above, the quenching model was not considered in more detail and the evaporative heat transfer model further refined. The bubble size and departure frequency, along with boiling area, were varied. Although the boiling area model in Eq. 21 includes an exponent  $p$ , which could also be varied, the exponent was found to affect convergence and have little influence on outputs of interest. The bubble size was split into two empirical parameters, a scaling ( $d_0$ ), and a temperature dependence ( $\Delta T_0$ ). Note that the inputs were not completely independent, since the departure frequency depends weakly on the bubble size.

Each of the four parameters was varied by  $\pm 30\%$ , and there were 472 converged runs on three meshes. The most significant effect was found to be the bubble size scaling  $d_0$ . Fig. 6 shows the strong correlation between pressure drop and  $d_0$ , which is verified by the correlation matrix in Table 3. Larger bubble sizes resulted in higher void fractions, lower pressure drops, and lower wall temperatures, as would be expected. In addition, the bubble size had the strongest effect on convergence. Of the 38 non-converged solutions, all except two had a  $d_0$  larger than the nominal value. Also, finer meshes and larger departure frequencies tended to lead to non-convergence.

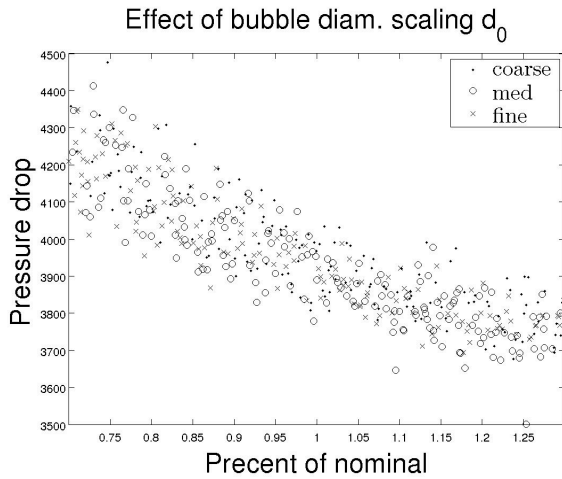


Figure 6. Effect of  $d_0$  on pressure drop

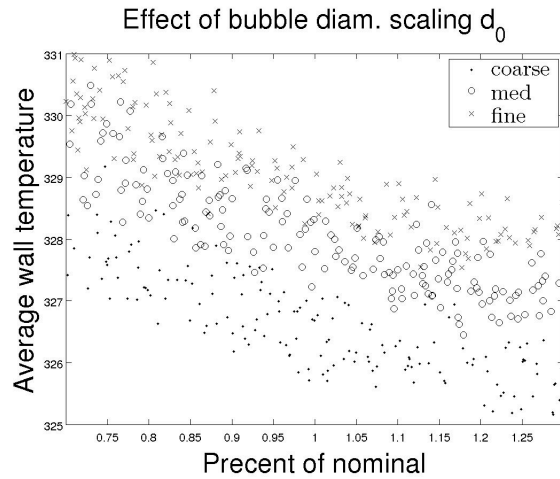


Figure 7. Effect of  $d_0$  on average wall temperature

	$n''$	$d_0$	$\Delta T_0$	$f$	mesh size
$\Delta p$	-0.350	-0.892	-0.135	-0.104	-0.003
$T_w$	-0.354	-0.855	-0.138	-0.209	0.736
$\alpha_g$	0.361	0.894	0.091	0.109	0.546

Table 3. Correlation of inputs and outputs

$\Delta p - T_w$	$\Delta p - \alpha_g$	$T_w - \alpha_g$
0.993	-0.998	-0.993

Table 4. Cross-correlation of outputs

As can be seen in Table 3, the bubble size temperature dependence parameter  $\Delta T_0$  was found to have very little effect on the outputs. This was likely due to the functional form of  $d_w$  in Eq. 28. In addition, the boiling area and departure frequency both had relatively small effects on the outputs. This was at least partially due to the fact that  $d_w$  enters cubically into  $q_T$ , whereas  $n''$  and  $f$  enter only linearly (see Fig. 3). Although boiling area had a significant effect in the three parameter study, here it was overshadowed by the strong influence of  $d_0$ .

As in the three parameter study, mesh size was not important for pressure drop but had a significant effect for the other outputs. For example, the average wall temperature is shown in Fig. 7. Despite this, Table 4 shows that all of the outputs were strongly correlated with each other, suggesting that the mesh dependence is not as strong as the parameter dependence.

## 6. Summary and Conclusions

This work presented a study of sensitivities of key outputs in a subcooled boiling benchmark problem, DEBORA, with respect to parameters that govern the wall-to-flow heat transfer model. A two-stage approach was followed in which sensitivities were computed first with respect to individual heat fluxes and second with respect to parameters in the models for these heat fluxes. Variations due to mesh resolution were also studied. Key conclusions are as follows: (1) the quenching heat flux has little effect on pressure drop, average wall temperature, and void fraction; (2) pressure drop is not strongly affected by mesh resolution, in contrast to the other two outputs; (3) boiling area and evaporative heat transfer have a strong affect on all three outputs; (4) in the evaporative heat transfer model, the bubble

size scaling  $d_0$  has the strongest effect on all three outputs and on convergence. These observations could be used to appropriately focus efforts for model improvement. Future work will consider sensitivities with respect to additional models, including those of phase-to-phase mass, momentum, and heat-transfer.

## 7. References

- [1] N. Kurul and M.Z. Podowski, “On the modelling of multidimensional effects in boiling channels,” ANS Proceedings, National Heat Transfer Conference, 1991.
- [2] R.M. Podowski and D.A. Drew and R.T. Lahey Jr. and M.Z. Podowski, “A Mechanistic Model of the Ebullition Cycle in Forced Convection Subcooled Boiling,” Proceedings of the 8<sup>th</sup> International Topical Meeting on Nuclear Reactor Thermal-Hydraulics. Vol. 3, 1997.
- [3] M.Z. Podowski, “Recent Development in the Modeling of Boiling Heat Transfer Mechanisms,” Proceedings of the 13<sup>th</sup> International Topical Meeting on Nuclear Reactor Thermal-Hydraulics, 2009.
- [4] G.H. Yeoh and J.Y. Tu “A Bubble Mechanistic Model for Subcooled Boiling Flow Predictions,” *Numerical Heat Transfer*, Vol 45, 2004, pp 475—493.
- [5] J.Y. Tu and G.H. Yeoh, “On numerical modelling of low-pressure subcooled boiling flows,” *International Journal of Heat and Mass Transfer*, Vol 45, 2002, pp 1197—1209.
- [6] Bostjan Koncar and Eckhard Krepper, “CFD Simulation of Convective Flow Boiling of Refrigerant in a Vertical Annulus,” *Nuclear Engineering and Design* 238, 2008, pp 693—706.
- [7] STAR-CD Version 4.14 Methodology Manual, Chapter 13, CD-adapco, 2010.
- [8] V. Ustinenko, M. Samigulin, A. Ioilev, S. Lo, A. Tentner, A. Lychagin, A. Razin, V. Girin, Ye. Vanyukov, “Validation of CFD-BWR, a new two-phase computational fluid dynamics model for boiling water analysis,” *Nuclear Engineering and Design* 238, 2008, pp 660-670.
- [9] Wang, D.M. 1994. ‘Modelling of bubbly flow in a sudden pipe expansion’, *Technical Report II-34*, BRITE/EuRam Project BE-4098.
- [10] Ranz, W.E., and Marshall, W.R. “Evaporation from drops — Parts I and II”, *Chem. Eng. Prog.*, 48(3), 1952, p. 141.
- [11] M. Ishii and T. Hibiki, *Thermo-Fluid Dynamics of Two-Phase Flow*, Springer 2006.
- [12] V.I. Tolubinsky and D.M. Kostanczuk, “Vapour Bubbles Growth Rate and Heat Transfer Intensity at Subcooled Water Boiling,” Proc. 4<sup>th</sup> International Heat Transfer Conference, Vol. 5, 1970.
- [13] J. Garnier, E. Manon, and G. Cubizolles, “Local Measurements on Flow Boiling of Refrigerant 12 in a Vertical Tube,” *Multiphase Science and Technology*, Vol. 13, 2001, pp.1-111.

**The 14<sup>th</sup> International Topical Meeting on Nuclear Reactor Thermalhydraulics, NURETH-14  
Toronto, Ontario, Canada, September 25-30, 2011**